Flexoelectric Cantilever Beam Mass Sensors: A Theoretical Investigation

Hossein Vaghefpour *

Department of Mechanical Engineering, Abadan Branch, Islamic Azad University, Abadan, Iran

ABSTRACT: This research explores a novel technique for precise mass sensing, involving the detection of an object's position and mass when affixed to a flexoelectric cantilever Euler-Bernoulli microbeam. Third-order relation of the curvature is considered to obtain the nonlinear governing equations and the related boundary conditions, from Hamilton's principle on the basis of size-dependent piezoelectricity theory. The Galerkin method is employed to discredit the partial differential equation of motion into ordinary differential equations. The Lindstedt-Poincare technique is employed to derive a concise mathematical expression that describes the frequency alteration resulting from the presence of a concentrated mass on the microbeam's exterior. By applying direct current voltage, the natural frequency shift of the flexoelectric cantilever Euler-Bernoulli microbeam under an added mass is examined. Finally, after validation of the results, the effects of size-dependent parameters, input voltage, and flexoelectric coefficient on static deformation and frequency behavior are shown. It can be found that the maximum sensitivity for l/h = 0.0 is at V0 = 2600v, By adjusting the material length scale factor relative to the beam thickness ratio, the sensitivity is observed to diminish. Also, by increasing the position of the added mass, the sensitivity is decreased and, where the flexoelectric effect is small, the increment in the position of added mass decreases the first and second frequency shift.

1- Introduction

The integration of Micro-Electro-Mechanical Systems (MEMS) and Nano-Electro-Mechanical Systems (NEMS) presents significant opportunities in various engineering disciplines, including mechanical, civil, and aerospace engineering. These technologies offer exceptional capabilities for precise measurement of physical parameters, such as minute gas concentrations, microscopic biological entities, and subtle variations in temperature and pressure [1]. Piezoelectric micro and nanobeams, in particular, have been extensively utilized within MEMS and NEMS as specialized piezoelectric sensors, actuators, energy harvesting [2], vibration control [3], vibration responses [4, 5], and positioning systems [6]. Particularly, flexoelectric cantilever micro and nanobeams have been developed with a novel micro/nano-electromechanical system process very useful for low-frequency vibration sensors and energy harvesters [7]. The application of micro-materials as active sensing particles in micro-sensors has increased the sensitivity performance of micro-sensors that can be able to detect particles, for example, bacteria with very nano-dimensions and low concentrations [8]. Also, micro and nanobeams are often implemented in the form of mass detector sensors of very small biological

and chemical species, such as viruses, bacteria, and cells [8]. Several methods e.g. static deflection and natural frequencies, have been used to measure the mass of very small elements, such as chemical and biological elements [9]. The static deflection method involves the detection of mass variations through precise measurements of microstructural deflections [9]. Another approach that is the more attractive method in terms of sensitivity, is frequency shift tracking. The frequency shift method, operating in dynamic mode, involves inducing vibrations in a microstructure, often a beam, near its natural frequency [10]. This technique is highly sensitive to mass variations on the microstructure's surface. When an additional mass is introduced, the altered beam mass causes a corresponding shift in its natural frequency. Ilic et al. utilized this principle to create a biosensor for detecting Escherichia coli, a pathogenic bacterium, by coating a microsensor with specific antibodies, thus demonstrating its potential in medical diagnostics and food safety monitoring [11]. Burg et al. [12] further advanced this concept by designing a suspended microchannel sensor that correlates the mass of particles within a microfluidic channel to the decrease in resonance frequency. Cantilever micro beams, in particular, have been extensively utilized in resonant mass sensors. Dohn et al. [13] investigated the sensitivity of such cantilever beam mass sensors, finding that maximum sensitivity occurs

*Corresponding author's email: h.vaghegpour@gmail.com

at the beam tip, and the added mass has minimal impact on the Q-factor damping. They also emphasized that employing multiple bending modes significantly enhances sensitivity. The exploration of flexoelectric micro beams as mass sensors offers promising advantages. Recent advancements in size-dependent theories have led to the development of higher-order continuum theories for micro and nano structures. These theories also incorporate electromechanical effects, leading to the formulation of size-dependent piezoelectricity and similar electromechanical theories.

However, in the micro and nanoscale some studies have depicted size-effect phenomena of piezoelectric solids and linear electromechanical coupling in isotropic dielectrics, the conventional piezoelectric theory fails to elucidate the size-dependent correlation between electric polarization and uniform strain in dielectric substances. [14]. On the other hand, dielectric polarization is influenced not solely by the strain tensor but also by the curvature tensor, adding complexity to the understanding of these materials. Therefore, it is necessary to develop a size-dependent piezoelectricity theory to employ the micro/nanostructures which is included by the curvature and the higher gradients of deformation. This size-dependent parameter for linear electromechanical coupling in isotropic dielectrics is called the flexoelectric effect [15]. Hence, it can be deduced that typically, the flexoelectric phenomenon can be found in all dielectrics. The study of size-dependent piezoelectricity has led to the development of various theories, addressing the complexities of deformation gradients [16] and rotation gradients within the context of couple stress theory [17]. This electromechanical approach, as presented in [18], reveals the unique behavior of materials at nanoscales, incorporating the size-dependent piezoelectric and flexoelectric effects influenced by mean curvature [18]. Building upon these theories, researchers have explored piezoelectric nanobeams, analyzing their mechanical and electrical properties [19]. Notably, Tadi [20] endeavored to formulate a comprehensive piezoelectric nanobeam model, utilizing the size-dependent piezoelectricity theory to capture the intricate behavior of these nanoscale structures. The flexoelectric micro beams are often used in MEMS devices as actuators.

The microactuators are designed to operate with either AC or DC voltage applications. When a DC voltage is applied, the actuator adjusts to a new equilibrium, resulting in a static deflection [21]. Numerous studies have investigated the nonlinear behavior of electrostatic micro-actuated beams under DC or combined AC-DC electrostatic actuation [22]. Flexoelectric microbeams, due to their distinct characteristics, can be employed as sensitive sensors for detecting minute masses, including viruses, bacteria, and cells with great accuracy [23]. Wu [24] by implementing the static deflection analysis, detects the mass of chemical and biological elements. In terms of sensitivity, a great attractive method is to operate a MEMS device in the vibration mode. In this case, a micro beam as a typical element of a MEMS device, is driven to vibrate around one of its natural frequencies [25]. Raiteri et

al. [26], studied the sensitivity of NEMS devices, specifically when they operate in a vibrational state near their natural frequencies. This investigation aligns with a comprehensive review of existing literature, which reveals a significant body of prior research centered on the phenomena of vibration, buckling, and static deflection in flexoelectric microbeams.

Also, investigation of changes in frequency has been limited to electrostatic sensors. Because of some advantages of employing flexoelectric micro beams instead of electrostatically micro beams, it can be considered as the most preferable for MEMS and NEMS. One can note that given that electrically conductive assemblies are composed of distinct components, namely the beam, and electrode, which are susceptible to detrimental elongation effects, the use of electrostatic actuators and sensors with a flexoelectric beam can be desirable.

In this paper, for the first time, an efficient model has been used to analyze a flexoelectric microtear as a mass sensor, and the effect of different parameters of the model on the measurement accuracy is shown with the help of different diagrams in the results section. A comprehensive investigation is required to explore the nonlinear frequency response of flexoelectric microstructures, particularly when considering the influence of minimal surface-absorbed mass and the application of direct current voltage. Hence, the objective of this paper is to use a nonlinear formulation for a flexoelectric cantilever micro Euler- Bernoulli beam is derived based on the size-dependent piezoelectricity theory, this study presents a comprehensive analysis of the flexoelectric cantilever micro beam's behavior under an applied voltage, utilizing the Hamilton principle. The focus is on deriving the nonlinear static deflection and vibration, considering the initial pre-static deformation. The Galerkin projection technique simplifies the governing partial differential equations to ordinary differential equations. Subsequently, the Lindstedt-Poincare perturbation method is employed to solve the resulting nonlinear ordinary differential equation. Following the validation of results, a detailed numerical investigation is performed to evaluate the frequency shifts in flexoelectric microbeam resonators due to the influence of added mass.

2- Governing Equations

This study investigates the potential of a microcantilever beam, composed of isotropic piezoelectric material, as a mass sensing device when exposed to a direct current (*DC*) voltage, V_{DC}, (Figure 1). The microcantilever mass sensor width, length, and thickness are, respectively, *b, L,* and *h*.

Based on size-dependent piezoelectricity, the strain energy of piezoelectric isotropic elastic materials with infinitesimal deformations occupying volume V is expressed as [14]:

$$U = \frac{1}{2}\lambda e_{jj}e_{kk} + \mu e_{ij}e_{ij} + 8\mu l^2 \kappa_i \kappa_j$$
$$-\frac{1}{2}\varepsilon E_i E_j - 4f E_i \kappa_i \tag{1}$$
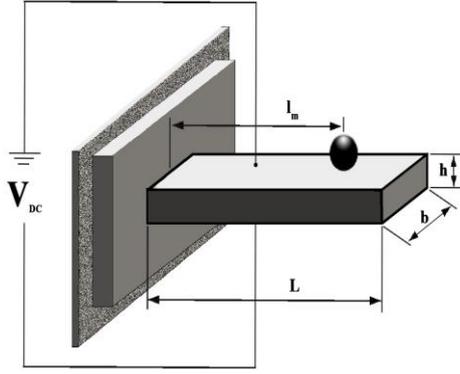
Fig. 1. Schema of an isotropic flexielectric micro-beam

where λ and μ are Lame's constants, and l, f, and ε are the size effect parameters, so called flexoelectric coefficient, dielectric constant (electric permittivity), and E_i stand for the electric field, respectively. By defining u_i as small displacement field in the continuum, e_{ij} and κ_i are defined, respectively, as [14]:

$$e_{ij} = \frac{1}{2}\left(u_i,_j + u_j,_i\right) \text{ and }$$
$$\kappa_i = \frac{1}{2}\left(u_k,_{ki} - \nabla^2 u_i\right) \tag{2}$$

If the position of a point on the elastic axis before deformation and after deformation is given by $\mathbf{r}_0 = s\mathbf{e}x$ and $\mathbf{r} = (s + u)\,\mathbf{e}_1 + w\mathbf{e}_3$ respectively, the strain along the elastic axis of a differential element *ds* is equal to [14]:

$$e = \left(\frac{\partial r}{\partial s}\cdot\frac{\partial r}{\partial s}\right)^{\frac{1}{2}} - \left(\frac{\partial r_0}{\partial s}\cdot\frac{\partial r_0}{\partial s}\right)^{\frac{1}{2}} = \sqrt{\left(1+u,_x\right)^2 + w,_x^2} - 1 \tag{3}$$

By assuming the inextensibility condition, the elongation eds become zero, therefore [27]:

$$\left(1+u,_x\right)^2 + w,_x^2 = 1 \tag{4}$$

Expanding the result of Eq. 3 in a Taylor expansion one can obtain [27]:

$$u,_x \approx -\frac{1}{2}w,_x^2 \tag{5}$$

The kinetic energy formulation for a flexoelectric

microstructure with an additional mass is derived from the displacement field, utilizing the Euler-Bernoulli beam theory as a foundational framework. [27]:

$$T = \frac{1}{2}\int_v \rho\left(u_{1,t}^2 + u_{2,t}^2 + u_{3,t}^2\right)dV + \frac{1}{2}m\delta\left(x - l_m\right)u_{3,t}^2 \tag{6}$$

Where ρ is the mass density of the microbeam, $\delta(x - l_m)$ is the Dirac delta function and m is the added point mass at $x = l_m$. The curvature relationship, expressed as a third-order equation, intricately links axial and transverse deformations, offering a comprehensive understanding of their intricate interplay [27]:

$$\rho^{(3)} = w,_{xx} - \left(u,_x w,_x\right),_x - w,_x^2 w,_{xx} \tag{7}$$

Substituting Eq. 5 into Eq. 7 and after some simplifications, the micro beam's kinetic energy and strain energy variations can be mathematically represented as distinct entities:

$$\int_{t_0}^{t_1}\left(\delta T\right)dt = \int_{t_0}^{t_1} - \int_0^L \left(F_{11}w,_{tt} - H_{11}w,_{ttxx}\right)\delta w\,dx$$
$$- m\delta\left(x - l_m\right)w,_{tt}\delta w\,dt$$
$$- \int_{t_0}^{t_1}H_{11}w,_{ttx}\delta w\Big|_0^L + m\delta\left(x - l_m\right)w,_t\delta w\Big|_0^L \tag{8}$$

And

$$U = \int_v\left(\sigma_{11}\delta e_{11} + 2\mu_{12}\delta\kappa_{21} - D_1\delta E_1 - D_3\delta E_3\right)dV$$
$$= \int_0^L EI w,_{xxxx} + w,_{xx}^3 + 3w,_x w,_{xx}w,_{xxx} + \frac{1}{2}w,_x^2 w,_{xxxx}\,\delta w\,dx$$
$$+ \int_0^L EI\left\{\left(w,_{xxx} + w,_x w,_{xx}^2 + \frac{1}{2}w,_x^2 w,_{xxx}\right)\frac{1}{2}w,_x^2\right\}\delta w\,dx$$
$$+ \int_0^L\left[A_{11}w,_{xx}\right],_{xx}\delta w\,dx\; EI\left(w,_{xx} + \frac{1}{2}w,_x^2 w,_{xx} + A_{11}w,_{xx}\right)\delta w,_x\Big|_0^L$$
$$- EI\left(w,_{xxx} + w,_x w,_{xx}^2 + \frac{1}{2}w,_x^2 w,_{xxx}\right)\delta w\Big|_0^L$$
$$EI\left[\left(w,_{xx} + \frac{1}{2}w,_x^2 w,_{xx}\right)\frac{1}{2}w,_x^2\right]\delta w,_x\Big|_0^L \tag{9}$$
$$- EI\left(w,_{xxx} + w,_x w,_{xx}^2 + \frac{1}{2}w,_x^2 w,_{xxx}\right)\frac{1}{2}w,_x^2\delta w\Big|_0^L$$
$$+ EI\left(w,_{xx}\frac{1}{2}w,_x^2 w,_{xx}\right)w,_x w,_{xxx}\delta w\Big|_0^L$$
$$EI\left[\left(w,_{xx} + \frac{1}{2}w,_x^2 w,_{xx}\right)w,_x w,_{xxx} - \left(A_{11}w,_{xx}\right),_x\right]\delta w\Big|_0^L$$

$$+\int \{\epsilon(\Phi_{,xx}+\Phi_{,zz})+2f_{,z}w_{,xx}\}\delta\Phi dV$$

$$-\int_{-b/2}^{b/2}\int_{-h/2}^{h/2}\epsilon\Phi_{,x}\delta\Phi dydz\Big|_{0}^{L}$$

$$-\int_{-b/2}^{b/2}\int_{0}^{L}(\epsilon\Phi_{,z}+2fw_{,x})\delta\Phi dydx\Big|_{-h/2}^{h/2}$$

$$-\int_{-b/2}^{b/2}\int_{0}^{L}(\epsilon\Phi_{,z}+2fw_{,x})\delta\Phi dydx\Big|_{-h/2}^{h/2}$$

In which

$$(F_{11},H_{11})=\int_{-b/2}^{b/2}\int_{-h/2}^{h/2}\tilde{n}(1,z^2),$$

$$I=\int_{-b/2}^{b/2}\int_{-h/2}^{h/2}z^2,$$

$$A_{11}=\int_{-b/2}^{b/2}\int_{-h/2}^{h/2}4\mu l^2 and$$

$$E_{11}=\int_{-b/2}^{b/2}\int_{-h/2}^{h/2}f(\Phi_{,z})dyd$$

Hamilton's principle is used to derive the equations of motion of the microbeam and the corresponding boundary conditions. [20]:

$$\delta w:(\lambda+2\mu)I\left(w_{,xxxx}+\left[w_{,x}(w_{,x}w_{,xx})_{,x}\right]_{,x}\right)$$
$$+A_{11}w_{,xxxx}-2(E_{11})_{,xx}+F_{12}w_{,tt}-H_{11}w_{,ttxx}=0 \tag{10}$$

$$\delta\Phi:\epsilon(\Phi_{,xx}+\Phi_{,zz})+2f_{,z}w_{,xx}=\rho_e \tag{11}$$

Where

$$F_{12}=\int_{-b/2}^{b/2}\int_{-h/2}^{h/2}\tilde{n}dydz+\frac{m}{L}\ddot{a}(x-l_m)$$

Neglecting the rotary inertia effect [28], i.e. H_{11}, and assuming $\rho_e=0$, the governing equations for a flexoelectric cantilever micro-beam system are presented in Eqs. 10 and 11, encompassing both mechanical and electrical boundary conditions. These equations provide a comprehensive framework to describe the intricate dynamics of such micro-scale structures.:

$$((\lambda+2\mu)I+A_{11})w_{,xxxx}$$
$$+(\lambda+2\mu)I\left[w_{,x}(w_{,x}w_{,xx})_{,x}\right]_{,x} \tag{12}$$
$$-2(E_{11})_{,xx}+F_{12}w_{,tt}=0$$

$$\epsilon(\Phi_{,xx}+\Phi_{,zz})+2f_{,z}w_{,xx}=0 \tag{13}$$

And

$$[((\lambda+2\mu)I+A_{11})w_{,xxx}$$
$$+(\lambda+2\mu)Iw_{,x}(w_{,x}w_{,xx})_{,x}-2(E_{11})_{,x}]\Big|_{0}^{L}=0 \tag{14}$$

$$[((\lambda+2\mu)I+A_{11})w_{,xx}$$
$$+(\lambda+2\mu)Iw_{,x}^2w_{,xx}-2(E_{11})]\big|_{0}^{L}=0 \tag{15}$$

$$\int_{A}(\Phi_{,x})dA=0 \quad or \quad \delta\Phi\Big|_{0}^{L}=0$$
$$\int_{A}\left[\Phi_{,z}+2f(w_{,xx})\right]dA=0 \quad or \tag{16}$$
$$\delta\Phi\Big|_{-\frac{h}{2}}^{\frac{h}{2}}=0$$

If the reverse effect of the electric potential is considered for the piezoelectric microbeam, the electric potential filed, i.e. Φ, and the electric field relationship respectively, is expressed by [29]:

$$\Phi(x,z,t)=\cos(\beta z)\Phi(x,t)+\frac{V_0(t)}{h}z \tag{17}$$

And [29]:

$$\mathbf{E}=-\nabla\Phi \quad i.e., \quad E_i=-\Phi_{,i} \tag{18}$$

Where $\beta=\frac{\pi}{h}$ and V_0 is the electric voltage which applied to the micro-beam. Through the application of Equation 17 within Equation 18, the electric potential field vector components are derived [29]:

$$\Phi_{,x}(x,z,t)=\cos(\beta z)\Phi_{,x}(x,t)\Phi_{,z}(x,z,t)=$$
$$-\beta\sin(\beta z)\Phi(x,t)+\frac{V_0(t)}{h} \tag{19}$$

By considering f to be a constant, $E_{11}=bf\ V_0$ and hence $(E_{11})_{,xx}=0$. Consequently, the equations of motion and their associated boundary conditions are transformed into the subsequent representation:

$$((\lambda+2\mu)I+A_{11})w_{,xxxx}+(\lambda+2\mu)$$
$$I\left[w_{,x}(w_{,x}w_{,xx})_{,x}\right]_{,x}+F_{12}w_{,tt}=0 \tag{20}$$

$$\delta w \big|_0 = 0 \quad \text{and} \left((\lambda+2\mu)I + A_{11} \right) w_{,xxx}$$
$$+ (\lambda+2\mu)I \left(w_{,x}^2 w_{,xxx} + w_{,x} w_{,xx}^2 \right) \big|^L = 0$$
$$\delta(w_{,x}) \big|_0 = 0 \quad \text{and} \tag{21}$$
$$\left((\lambda+2\mu)I + A_{11} \right) w_{,xx} + (\lambda+2\mu)I w_{,x}^2 w_{,xx}$$
$$- 2bfV_0(t) \big|^L = 0$$

For convenience, the following nondimensional variables are introduced as [30]:

$$\bar{w} = \frac{w}{L}$$
$$\bar{x} = \frac{x}{L}$$
$$\tau = t \sqrt{\frac{(\lambda+2\mu)I}{\rho A L^4}} \tag{22}$$
$$\bar{l}_m = \frac{l_m}{L}$$

Upon simplifying the notation $\overline{(\cdot)}$, the governing equation for the flexoelectric cantilever micro sensor (FCMS) can be represented in non-dimensional form, accompanied by its respective boundary conditions.

$$\left(1 + \alpha\delta(x - l_m) \right) w_{,\tau\tau} + L_s w_{,xxxx}$$
$$+ w_{,x}^{s\,2} w_{,xxxx} + w_{,xxxx}^s w_{,x}^2 + w_{,x}^2 w_{,xxxx}$$
$$+ 2w_{,x}^2 w_{,xxxx}^s w_{,x} + 2w_{,x}^s w_{,xxxx} w_{,x}$$
$$+ 4(w_{,x}^s w_{,xx}^s w_{,xxx} + w_{,x}^s w_{,xxx}^s w_{,xx}$$
$$+ w_{,x}^s w_{,xxx} w_{,xx} + w_{,xx}^s w_{,xxx}^s w_{,x} \tag{23}$$
$$+ w_{,xx}^s w_{,xxx} w_{,x} + w_{,xx}^s w_{,xx} w_{,x}$$
$$+ w_{,xxx} w_{,xx} w_{,x}) + 3w_{,xx}^{s\,2} w_{,xx}$$
$$+ 3w_{,xx}^{s\,2} w_{,xx}^2 + w_{,xx}^3 = 0$$

In Eq. 23 d superscript, due to brevity, is omitted.

3- Galerkin Approximate Method

The Galerkin projection method is employed to discretize the nonlinear dynamic equations of motion, specifically Equation 23. This approach enables the approximation of the complex nonlinear vibration behavior exhibited by the flexoelectric microsensor [31]:

$$w = \sum_{i=1}^{n} \psi_i(x) q_i(t) \tag{24}$$

where the $q_i(t)$ and $\psi i(x)$ are the ith generalized displacement coordinate, and the ith linear normal mode of a cantilever beam respectively, given by [31]:

$$\psi_i(x) = \cosh(r_i x) - \cos(r_i x)$$
$$+ \frac{\cos(r_i) + \cosh(r_i)}{\sin(r_i) + \sinh(r_i)} \tag{25}$$
$$\left(\sin(r_i x) - \sinh(r_i x) \right)$$

where r_i is the ith root of the characteristic equation for clamped-free beams given by $cos(r)\,cosh(r) = -1$. By substituting Equation 24 into the nonlinear transverse equation of motion, represented by Equation 23, and employing the Galerkin method, we derive a reduced-order model of the equation of motion:

$$\ddot{q}_k(t) + \alpha_{3,k} q_k(t)^3 +$$
$$\alpha_{2,k} q_k^2(t) + \alpha_{1,k} q_k(t) = 0 \tag{26}$$
$$q_k(0) = a_0 \quad \dot{q}_k(0) = 0$$

where $\alpha_{3,k}$, $\alpha_{2,k}$ and $\alpha_{1,k}$ are given, respectively, by:

$$\alpha_{3,k} = \frac{1}{1 + \alpha\psi_j^2(l_m)} \left[\xi_{1,k} + \xi_{2,k} + 4\xi_{3,k} \right],$$
$$\alpha_{2,k} \frac{1}{1 + \alpha\psi_j^2(l_m)} = 2\xi_{4,k} + 4\xi_{5,k} + 4\xi_{6,k}$$
$$+ 4\xi_{7,k} + 3\xi_{8,k} + \xi_{9,k}, \tag{27}$$
$$\alpha_{1,k} \frac{1}{1 + \alpha\psi_j^2(l_m)} = 2\xi_{10,k} + L_s \xi_{11,k} + 4\xi_{12,k}$$
$$+ 4\xi_{13,k} + 4\xi_{14,k} + \xi_{15,k} + 3\xi_{16,k},$$

In which $\xi_{1,k}$ to $\xi_{16,k}$ relations are:

$$\xi_{1,k} = \int_0^1 \psi_k(x) \psi_k''^3(x) dx$$
$$\xi_{2,k} = \int_0^1 \psi_k(x) \psi_k'^2(x) \psi_k^{(4)}(x) dx$$
$$\xi_{3,k} = \int_0^1 \psi_k(x) \psi_k'(x) \psi_k''(x) \psi_k'''(x) dx$$
$$\xi_{4,k} = \int_0^1 \psi_k(x) w^{s'} \psi_k'(x) \xi_i^4(x) dx \tag{28}$$
$$\xi_{5,k} = \int_0^1 \psi_k(x) w^{s'} \psi_k''(x) \psi_k''(x) dx$$
$$\xi_{6,k} = \int_0^1 \psi_k(x) w^{s''} \psi_k'(x) \psi_k''(x) dx$$
$$\xi_{7,k} = \int_0^1 \psi_k(x) w^{s'''} \psi_k'(x) \psi_k''(x) dx$$

$$\xi_{8,k} = \int_0^1 \psi_k(x) w^{s"} \psi_k^{"2}(x) dx$$

$$\xi_{9,k} = \int_0^1 \psi_k(x) w^{s(4)} \psi_k^{'2}(x) dx$$

$$\xi_{10,k} = \int_0^1 \psi_k(x) w^{s'} w^{s(4)} \psi_k^{'}(x) dx$$

$$\xi_{11,k} = \int_0^1 \psi_k(x) \psi_k^{(4)}(x) dx$$

$$\xi_{12,k} = \int_0^1 \psi_k(x) w^{s'} w^{s"} \psi_k^{"}(x) dx$$

$$\xi_{13,k} = \int_0^1 \psi_k(x) w^{s'} w^{s"'} \psi_k^{"}(x) dx$$

$$\xi_{14,k} = \int_0^1 \psi_k(x) w^{s"} w^{s"'} \psi_k^{'}(x) dx$$

$$\xi_{15,k} = \int_0^1 \psi_k(x) w^{s'2} \psi_k^{(4)}(x) dx$$

$$\xi_{16,k} = \int_0^1 \psi_k(x) w^{s'2} \psi_k^{"}(x) dx$$

4- Perturbation Technique Journal

This study utilizes the Lindstedt-Poincare perturbation method to derive a closed-form formula for calculating the microbeam's natural frequency shifts caused by additional mass, as presented in Equation 23. In this context, the generalized coordinate is denoted as $q_k(t,\varepsilon) = \varepsilon x_1(\tau) + \varepsilon^2 x_2(\tau) + \varepsilon^3 x_3(\tau)$, where ε represents a bookkeeping parameter employed in perturbation techniques to organize variables systematically. $\tau = \omega_k^{NL}(\in)t\,\omega_k^{NL}$ is the k_{th} nonlinear frequency, as derived in [32] $\omega_k^{NL}(\in) = \omega_k + \in\omega_{1,k} + \in^2\omega_{2,k} + \in^3\omega_{3,k}$, is expressed in terms of ω_k, the k_{th} linear natural frequency, and $\omega_{i,k}$, which are determined during the solution process. Inserting this generalized coordinate into Equation (26) yields a subsequent expression.

$$
\begin{aligned}
&\left(\omega_k + \epsilon\omega_{1,k} + \epsilon^2\omega_{2,k}\right)^2 \frac{d^2}{d\tau^2}\left(\epsilon x_1 + \epsilon^2 x_2 + \epsilon^3 x_3\right) \\
&+ \alpha_{1,k}\left(\epsilon x_1 + \epsilon^2 x_2 + \epsilon^3 x_3\right)^1 \\
&+ \alpha_{2,k}\left(\epsilon x_1 + \epsilon^2 x_2 + \epsilon^3 x_3\right)^2 \\
&+ \alpha_{3,k}\left(\epsilon x_1 + \epsilon^2 x_2 + \epsilon^3 x_3\right)^3 = 0
\end{aligned}
\tag{29}
$$

It follows from Eq. 29 and some simplifications, that the frequency shift due to the added mass of the FCMS is given by [31]:

$$\Delta\omega_k = \omega_k^{NL} - \omega_k = \frac{1}{4}\left(\frac{\left(9\alpha_{3,k}\omega_k^2 - 10\alpha_{2,k}^2\right)}{6\omega_k^3}\right)a_k^2 \tag{30}$$

5- Numerical results and discussion

The flexoelectric phenomenon is a crucial aspect at the micro and nanoscopic levels, warranting further investigation. To elucidate this, we examine a flexoelectric cantilever microsensor composed of BaTiO3, with its geometric and material characteristics detailed in Table 1.

To verify the current results, the obtained Galerkin outcomes for the nonlinear static deflection due to a DC voltage without added mass are compared with the available linear analytical results which is accessible in Ref. [33], and the current *bvp4c* results. The comparison is depicted in Fig. 2 for $V_0 = 4000v$ by the consideration of 1 and 3 linear normal modes in Galerkin projection. A very good agreement is clear between the current 3-mode Galerkin projection, the *bvp4c* method, and the analytical results. Because the Galerkin approach is very handyin the implementation hence, hereafter 3-mode Galerkin technique is employed for the static deflection computations.

Table 1. The geometrical and material data of the assumed piezoelectric nanobeam [20].

Parameter	Description	Value (Unit)
L	Beam Length	50 (μm)
b	Beam Width	2 (μm)
h	Beam Thickness	1 (μm)
l	Scale factor	0.2h
f	Flexoelectric Coefficient	5e−9 (C/m)
μ	Lame Constant	42.9 (GPa)
λ	Lame Constant	45.2 (GPa)
ρ	Density	4000 (Kg/m3)
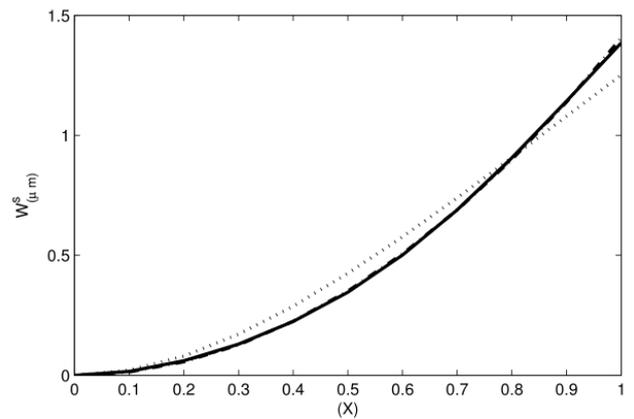
Fig. 2. Nonlinear static deflection of the proposed model with first-order Galerkin (dotted lines), third-order Galerkin (solid lines), and bvp4c subroutine (dashed lines) versus the corresponding linear analytical results of Ref. [33] (dotted lines): (V0 = 4000v).

Table 2. Comparison of the first natural frequency of the current model with reference results [34] (MHz)

| Natural Frequency	Ref. [30]	Current Model	Difference %
ω_1	0.3108	0.3107	0.03
ω_1	1.9326	1.9468	0.73

Also, another validation for the natural frequency of the current model with reference [34] is given in Table 2. The model presented in [34] for a rotating macro beam made of epoxy with $E=1.4$ Gpa, $\upsilon=0.3$, $\rho=1220$ kg/m^3, and $l=17.6$ μm, where ρ is beam density, υ is Poisson's coefficient, E is elastic modulus and l is size factor. Considering that the beam studied in reference [34] is a rotating beam, to compare the linear frequencies with the present model, in reference [34], $\lambda\_R=0$ is considered and in the current model, the mass value is considered to be zero. Table 2 presents a comparative analysis of the initial two natural frequencies, revealing a high degree of consistency in the outcomes. Notably, this alignment is observed when contrasted with the reference data [34], the results were obtained by considering the effect of rotational inertia, while this effect was omitted in this research.

After validation, the effect of other parameters will be examined.

The variation of the first, second and third natural frequency with respect to the position of the added mass for different effects of the length scale parameter to the beam thickness ratio, i.e. l/h are demonstrated in Figs. 3- 5. It can be seen that by increasing l/h parameter due to the stiffening of the beam structure the natural frequencies increase. Also, the maximum frequency is at $l_m = 1$, $l_m = 0.78$ and $l_m = 0.5$ for the first, second, and third natural frequency, respectively.
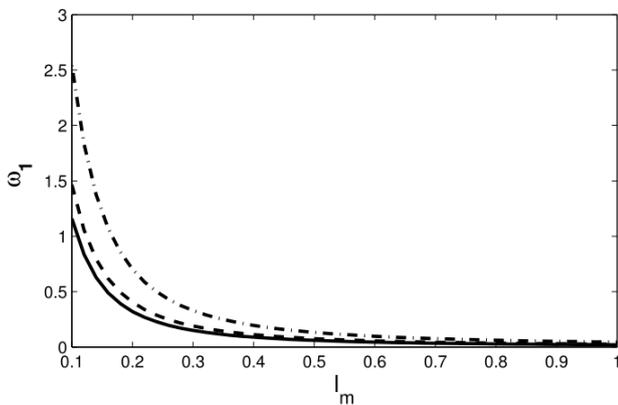
Fig. 3. The first frequency of FCMS for different the effect of the length scale parameter to the beam thickness ratio, i.e. l/h: l/h = 0.0, solid-lines, l/h = 0.2, dashed-lines, and l/h = 0.5, dotted-dashed-lines.
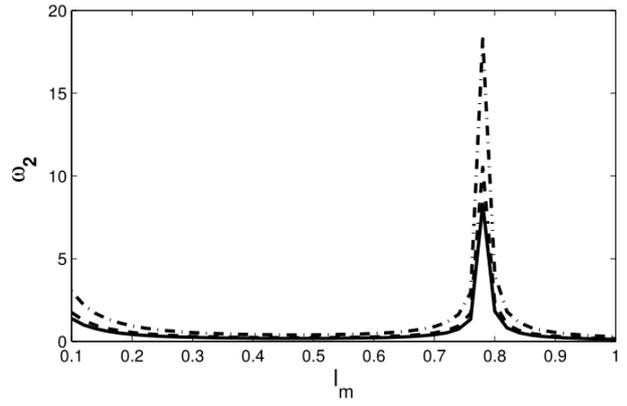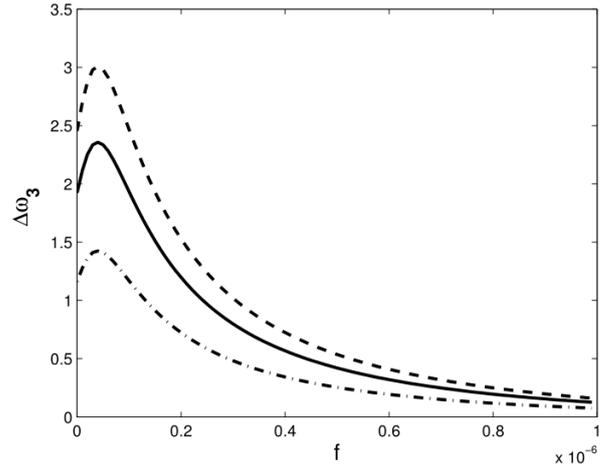

Fig. 4. The second frequency of FCMS for different the effect of the length scale parameter to the beam thickness ratio, i.e. l/h: l/h = 0.0, solid-lines, l/h = 0.2, dashed-lines, and l/h = 0.5, dotted-dashed-lines
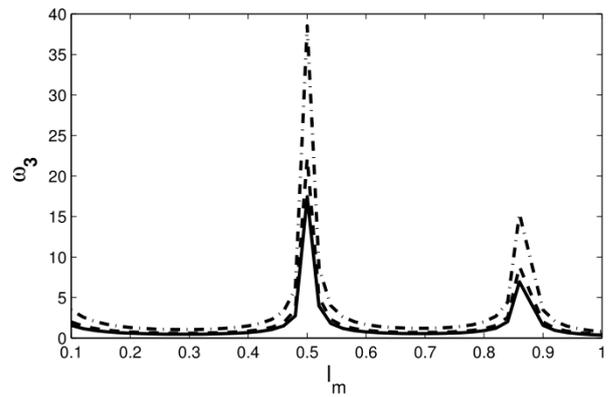
Fig. 5. The third frequency of FCMS for different the effect of the length scale parameter to the beam thickness ratio, i.e. l/h: l/h = 0.0, solid-lines, l/h = 0.2, dashed-lines, and l/h = 0.5, dotted-dashed-lines

The first, second, and third frequency shifts of the FCMS which undergoes different flexoelectric coefficients as a function of the position of the added mass are illustrated in Figs. 6-8. It can be seen that (Figs. 6 and 7) the first and second frequency shifts are decreased by increasing the position of the added mass in thesmall flexoelectric coefficient. But by increasing the flexoelectric coefficient, because of the softening behavior [30], the first and second frequency shift are increased by increasing the position of the added mass. In the context of the fexoelectric constant, the third frequency shift of the FCMS consistently indicates a hardening trend, as illustrated
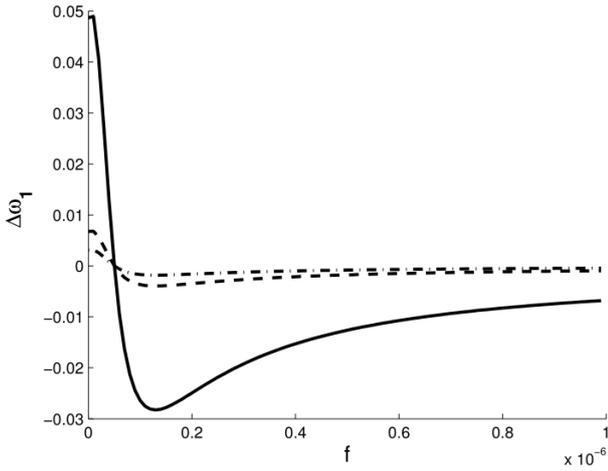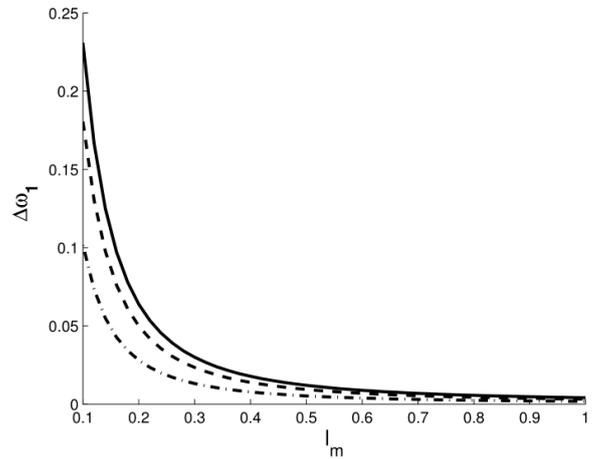
Fig. 6. The first frequency shift of FCMS for different position of the added mass: lm = 0.2L, solid-lines, lm = 0.6L, dashed-lines, and lm = L, dotted-dashed-lines

Fig. 8. The third frequency shift of FCMS for different position of the added mass: lm = 0.2L, solid-lines, lm = 0.6L, dashed-lines, and lm = L, dotted-dashed-lines
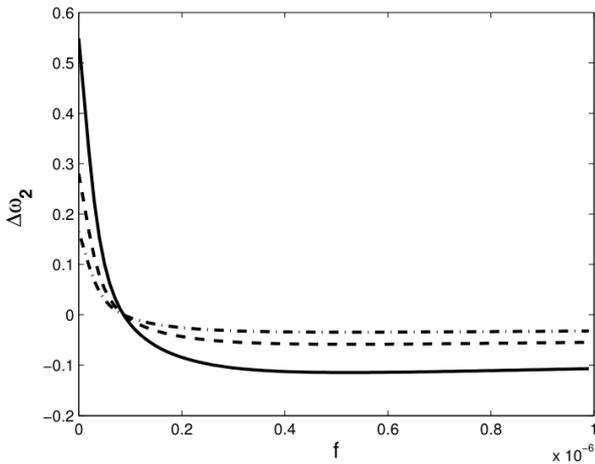
Fig. 7. The second frequency shift of FCMS for different positions of the added mass: lm = 0.2L, solid-lines, lm = 0.6L, dashed-lines, and lm = L, dotted-dashed-lines

Fig. 9. The first frequency shift of FCMS for different effect of the material length scale factor with respect to the beam thickness ratio: l/h = 0.0, solid-lines, l/h = 0.2L, dashed-lines, and l/h = 0.5, dotted-dashed-lines

in Figure 8. Figures 9- 11 illustrate the first, second, and third frequency shift of the FCMS under different positions of the added mass, as a function of the effect of the lengthscale parameter to the beam thickness ratio, i.e. l/h. Figs. 9- 11 show, by increasing l/h, the frequency shifts are decrease. Also, in Figs. 9- 11 One can note that the maximum frequency shifts are at $lm = 1$, $lm = 0.78$ and $lm = 0.5$ for the first, second, and third frequency shifts, respectively.

The similar study as the frequency shift under *DC* voltage are performed for the sensitivity respectively, in Figs. 12- 14. From Fig. 12 it can be inferred that the maximum sensitivity

is at $V_0 = 2600v$ for $l/h = 0.0$ and more than $V_0 = 4000v$ for $l/h = 0.2$. The comparison of the fig. 12 and fig. 13 shows that by increasing the material length scale factor with respect to the beam thickness ratio: l/h the sensitivity is decrease.
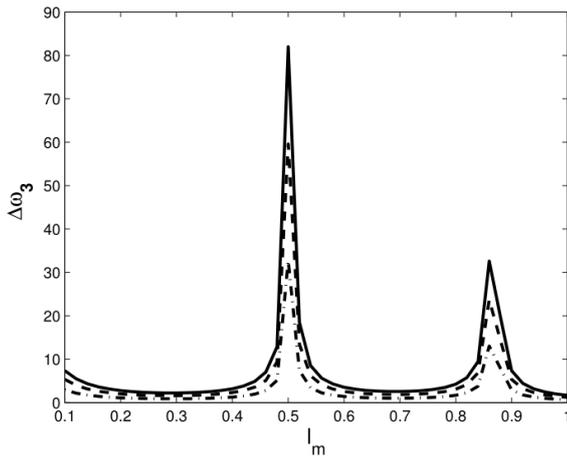
Also, by comparison of Fig. 14 and Fig. 15 it can be deduced that by increasing the position of the added mass l_m the sensitivity is decreased.

6- Conclusions

This study investigates the frequency shifts of a micro-cantilever beam with an attached point mass, utilizing a pre-actuated isotropic design. The analysis is based on the
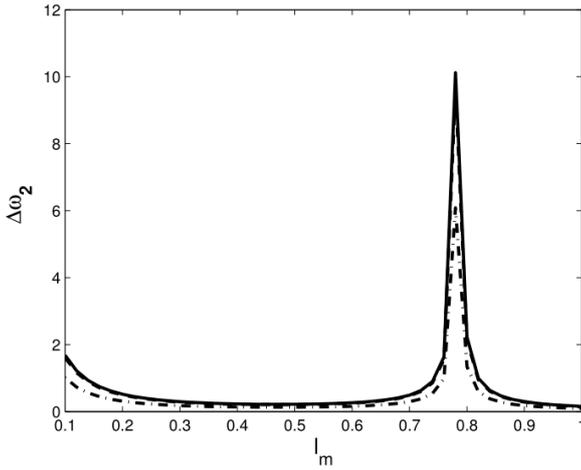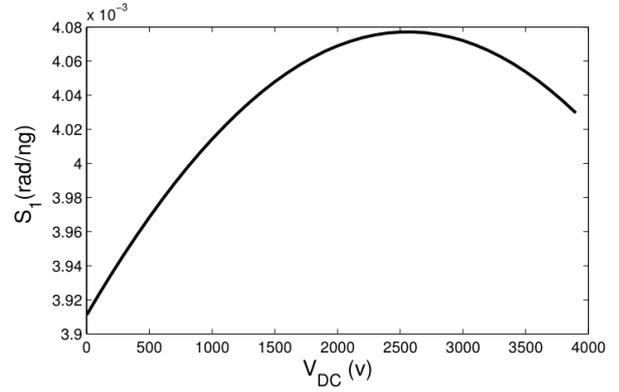
Fig. 10. The second frequency shift of FCMS for the different effect of the material length scale factor with respect to the beam thickness ratio: l/h = 0.0, solid-lines, l/h = 0.2L, dashed-lines, and l/h = 0.5, dotted-dashed-lines

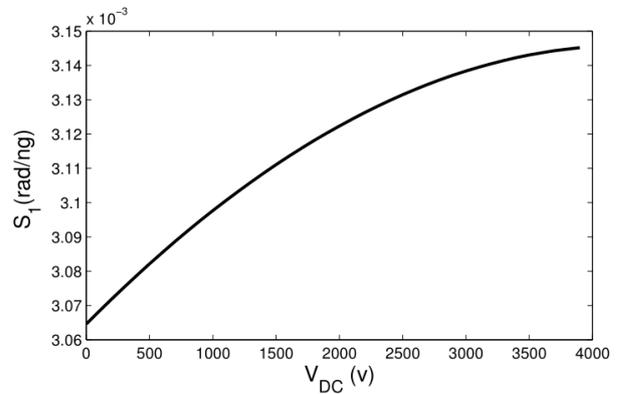**Fig. 12. The sensitivity in terms of applied DC voltage for l/h = 0**

Fig. 11. The third frequency shift of FCMS for different effect of the material length scale factor with respect to the beam thickness ratio: l/h = 0.0, solid-lines, l/h = 0.2L, dashed-lines, and l/h = 0.5, dotted-dashed-lines

Fig. 13. The sensitivity in terms of applied DC voltage for l/h = 0.2

Fig. 14. The sensitivity in terms of applied DC voltage for position of the added mass lm = 1
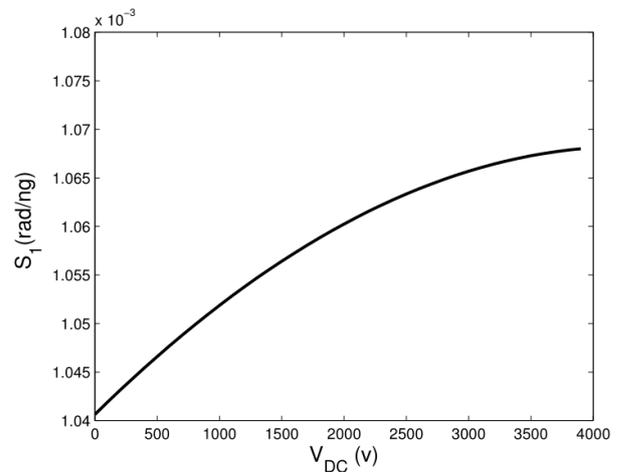
Euler-Bernoulli beam theory, derived from the Hamilton principle, and incorporates size-dependent piezoelectric effects. Given the negligible size of the added mass relative to the beam length, a high-order curvature displacement relationship was formulated. Through the application of Galerkin approximation and Lindstedt-Poincare perturbation methods, analytical expressions were derived to determine frequency shifts, considering variables such as added mass position, DC voltage, material length scale, and flexoelectric coefficient. These expressions elucidate the influence of these parameters on the linear natural frequency, frequency shifts, and sensitivity. The main
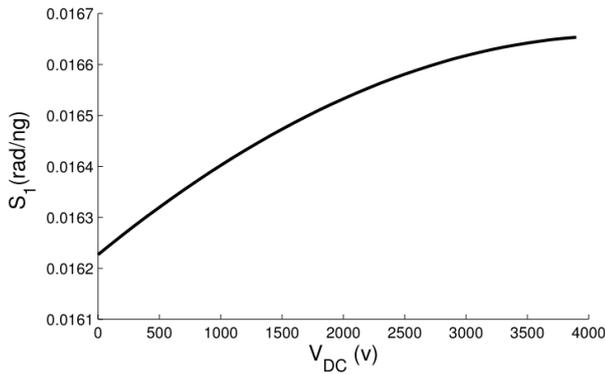
Fig. 15. The sensitivity in terms of applied DC voltage for the position of the added mass lm = 0.2L

findings are as follows:

The increment in the scale factor to the beam thickness ratio increases the linear natural frequency;

In the small flexoelectric region, the increment in the position of added mass decreases the first and second frequency shifts;

The increment in the scale factor to the beam thickness ratio decreases the frequency shifts;

The maximum sensitivity for *l/h = 0.0* is at $V_0 = 2600v$;

By increasing the material length scale factor with respect to the beam thickness ratio, the sensitivity is decreased;

By increasing the position of the added mass, the sensitivity is decreased.

References

[1] M. Baghelani, A. Hosseini-Sianaki, Z. Behzadi, A. Lavasani, Simulation of capacitive pressure sensor based on microelectromechanical systems technology, Proceedings of the Institution of Mechanical Engineers, Part C: Journal of Mechanical Engineering Science, 232 (2017) 095440621770609.

[2] S. Faroughi, E.F. Rojas, A. Abdelkefi, Y.H. Park, Reduced-order modeling and usefulness of non-uniform beams for flexoelectric energy harvesting applications, Acta Mechanica, 230(7) (2019) 2339-2361.

[3] M. Fan, H. Tzou, Vibration control with the converse flexoelectric effect on the laminated beams, Journal of Intelligent Material Systems and Structures, 30 (2019) 1045389X1984401.

[4] A. Moura, Combined piezoelectric and flexoelectric effects in resonant dynamics of nanocantilevers, Journal of Intelligent Material Systems and Structures, 29 (2018) 1045389X1880344.

[5] D.-P. Zhang, Y. Lei, S. Adhikari, Flexoelectric effect on vibration responses of piezoelectric nanobeams embedded in viscoelastic medium based on nonlocal elasticity theory, Acta Mechanica, 229 (2018).

[6] J. Li, H. Huang, T. Morita, Stepping piezoelectric actuators with large working stroke for nano-positioning systems: A review, Sensors and Actuators A: Physical, 292 (2019) 39-51.

[7] S.F. Dehkordi, Y.T. Beni, On the size-dependent electromechanical layered beam-type porous functionally graded flexoelectric energy harvesters, Engineering Analysis with Boundary Elements, 165 (2024) 105801.

[8] P. Joshi, S. Kumar, V. Jain, J. Singh, Distributed MEMS Mass-Sensor Based on Piezoelectric Resonant Micro-Cantilevers, Journal of Microelectromechanical Systems, PP (2019).

[9] E. Habibi, M. Nematollahi, Position and mass identification in nanotube mass sensor using neural networks, Proceedings of the Institution of Mechanical Engineers, Part C: Journal of Mechanical Engineering Science, 233 (2019) 095440621984107.

[10] K.M. Hansen, T. Thundat, Microcantilever biosensors, Methods (San Diego, Calif.), 37(1) (2005) 57-64.

[11] B. Ilic, H.G. Craighead, S. Krylov, W.Senarante, C. Ober, O.Neuzil, Attogram detection using nanoelectromechanical oscillators, Journal of Applied Physics, 95 (2004).

[12] T. Burg, A. Mirza, N. Milovic, C. Tsau, G. Popescu, J. Foster, S. Manalis, Vacuum-Packaged Suspended Microchannel Resonant Mass Sensor for Biomolecular Detection, Microelectromechanical Systems, Journal of, 15 (2007) 1466-1476.

[13] S. Dohn, R. Sandberg, W. Svendsen, A. Boisen, Enhanced functionality of cantilever based mass sensors using higher modes and functionalized particles, 2005.

[14] A.R. Hadjesfandiari, Size-dependent piezoelectricity, International Journal of Solids and Structures, 50(18) (2013) 2781-2791.

[15] S. Dehkordi, Y. Tadi Beni, Electro-mechanical free vibration of single-walled piezoelectric/flexoelectric nano cones using consistent couple stress theory, International Journal of Mechanical Sciences, 128 (2017).

[16] R. Maranganti, N.D. Sharma, P. Sharma, Electromechanical coupling in nonpiezoelectric materials due to nanoscale nonlocal size effects: Green's function solutions and embedded inclusions, Physical Review B - PHYS REV B, 74 (2006).

[17] G.-F. Wang, S.-W. Yu, X.-Q. Feng, A piezoelectric constitutive theory with rotation gradient effects, European Journal of Mechanics - A/Solids, 23(3) (2004) 455-466.

[18] A. Hadjesfandiari, G. Dargush, Couple stress theory for solids, International Journal of Solids and Structures - INT J SOLIDS STRUCT, 48 (2011) 2496-2510.

[19] Z. Yan, L. Jiang, Size-dependent bending and vibration behavior of piezoelectric nanobeams due to flexoelectricity, Journal of Physics D: Applied Physics, 46 (2013) 355502.

[20] [20] Y. Tadi Beni, A Nonlinear Electro-Mechanical Analysis of Nanobeams Based on the Size-Dependent Piezoelectricity Theory, Journal of Mechanics, -1 (2016) 1-13.

[21] A. Bouchaala, A. Nayfeh, N. Jaber, M. Younis, Mass and position determination in MEMS mass sensors: A theoretical and an experimental investigation, Journal of Micromechanics and Microengineering, 26 (2016).

[22] M. Shaat, S.A. Mohamed, Nonlinear-electrostatic analysis of micro-actuated beams based on couple stress and surface elasticity theories, International Journal of Mechanical Sciences, 84 (2014) 208-217.

[23] K. Park, L.J. Millet, N. Kim, H. Li, X. Jin, G. Popescu, N.R. Aluru, K.J. Hsia, R. Bashir, Measurement of adherent cell mass and growth, Proceedings of the National Academy of Sciences, 107(48) (2010) 20691-20696.

[24] G. Wu, R.H. Datar, K.M. Hansen, T. Thundat, R.J. Cote, A. Majumdar, Bioassay of prostate-specific antigen (PSA) using microcantilevers, Nature biotechnology, 19(9) (2001) 856-860.

[25] L.G. Carrascosa, M. Moreno, M. Álvarez, L.M. Lechuga, Nanomechanical biosensors: a new sensing tool, TrAC Trends in Analytical Chemistry, 25(3) (2006) 196-206.

[26] R. Raiteri, M. Grattarola, H.-J. Butt, P. Skládal, Micromechanical cantilever-based biosensors, Sensors and Actuators B: Chemical, 79(2) (2001) 115-126.

[27] W. Lacarbonara, Nonlinear Structural Mechanics Nonlinear Structural Mechanics. Theory, Dynamical Phenomena and Modeling, 2013.

[28] A. Najafi Sohi, P.M. Nieva, Size-dependent effects of surface stress on resonance behavior of microcantilever-based sensors, Sensors, and Actuators A: Physical, 269 (2018) 505-514.

[29] Y. Solyaev, S. Lurie, Pure bending of a piezoelectric layer in second gradient electroelasticity theory, Acta Mechanica, 230 (2019).

[30] H. Vaghefpour, H. Arvin, Nonlinear free vibration analysis of pre-actuated isotropic piezoelectric cantilever Nano-beams, Microsystem Technologies, 25 (2019).

[31] M.I. Younis, A.H. Nayfeh, A Study of the Nonlinear Response of a Resonant Microbeam to an Electric Actuation, Nonlinear Dynamics, 31 (2003) 91-117.

[32] A. Barari, H. Dadashpour Kaliji, M. Ghadimi, D. domiri ganji, Non-Linear Vibration of Euler-Bernoulli Beams, Latin American Journal of Solids and Structures, 8 (2011) 139-148.

[33] Y. Tadi Beni, Size-dependent electromechanical bending, buckling, and free vibration analysis of functionally graded piezoelectric nanobeams, Journal of Intelligent Material Systems and Structures, 27 (2016).

[34] H. Arvin, Free vibration analysis of micro rotating beams based on the strain gradient theory using the differential transform method: Timoshenko versus Euler-Bernoulli beam models, European Journal of Mechanics - A/Solids, 65 (2017).